# Advanced Trajectory Engineering of Diffraction-Resisting Laser Beams

Ioannis D. Chremmos[1], Zhigang Chen[2], Demetrios N. Christodoulides[3] and Nikolaos K. Efremidis[1]

[1]*Department of Applied Mathematics, University of Crete, Heraklion 71409, Greece*
[2]*Department of Physics and Astronomy, San Francisco State University, San Francisco, California 94132, U.S.A.*
[3]*CREOL/ College of Optics, University of Central Florida, Orlando, Florida 32816, U.S.A.*

Keywords:     Laser Beams, Bessel Beams, Diffractionless Beams, Accelerating Beams, Trajectory Engineering.

Abstract:     We introduce an analytical technique for engineering the trajectory of diffraction-resisting laser beams. The generated beams have a Bessel-like transverse field distribution and can be navigated along rather arbitrary curved paths in free space, thus being an advanced hybrid between accelerating and non-accelerating diffraction-free optical waves. The method involves phase-modulating the wavefront of a Gaussian laser beam to create a continuum of conical ray bundles whose apexes define a prespecified focal curve, along which a nearly perfect circular intensity lobe propagates without diffracting. Through extensive numerical simulations, we demonstrate the great flexibility in the design of a gamut of different beam trajectories. Propagation around obstructions and self-healing scenarios are also investigated. The proposed wave entities can be used extensively for light trajectory control in applications such as laser microfabrication, optical tweezers and curved plasma filamentation spectroscopy.

## 1 INTRODUCTION

Over the past few years there has been a vivid interest in optical beams with peculiar diffraction and propagation properties. The stimulus has been the broad set of new possibilities and disciplines in optical micromanipulation, testing and manufacturing enabled by our ability to navigate the optical power on appropriately 'sculpted' optical waveforms (Grier, 2003); (Andrews, 2008). Such structured optical beams can be used to overcome the diffraction limitations in focusing optical power at long distances and, moreover, to control the trajectory of light around obstructions and provide access to otherwise inaccessible regions of the medium being tested or processed.

Structured laser beams with such advantageous characteristics can so far be distinguished into two major categories: *non-accelerating* and *accelerating*. The first category includes the classical diffraction-free solutions of Maxwell's equations whose profile and direction of propagation remains invariant as they evolve in space. Bessel beams (Durnin, 1987) are arguably the most widely known members of this family and perhaps the only propagation-invariant beams that have actually been used in applications successfully (Durnin et al., 1987); (Herman and Wiggins, 1991). This is owed to their simple structure, essentially being the result of interference of a conical bundle of plane waves, that can be easily obtained by passing a broad Gaussian laser beam through a conical lens, the axicon (Arlt and Dholakia, 2000); (Herman and Wiggins, 1991). The indirect generation of Bessel beams in the Fourier domain is also straightforward due to the simple annular shape of their Fourier transform (Durnin et al., 1987). Since their inception, Bessel beams have found diverse applications in micromanipulation, atom and nonlinear optics (McGloin and Dholakia, 2005). Other less known types of non-accelerating diffractionless waves exist, such as parabolic (Bandres et al., 2004) and Mathieu (Gutiérrez-Vega et al., 2000) waves; however they haven't been used in applications so far due to the complicated structure of their wavefront.

The second category involves optical beams whose profile remains invariant along a transversely accelerating frame of coordinates. The existence of these beams was revealed in 2007 when the quantum-mechanics concept of the Airy wavepacket

(Berry and Balazs, 1979) was introduced into the optics domain by Siviloglou and Christodoulides (2007). Airy optical beams were the first diffraction-free beams with the ability to self-accelerate along a parabolic trajectory in free space. The implementation of realistic, finite-energy Airy optical wavepackets was also found to be straightforward after it was found that the Fourier transform of the exponentially truncated Airy function is a Gaussian modulated by a cubic phase (Siviloglou and Christodoulides, 2007). Soon after their conception, these finite energy Airy beam counterparts were generated and demonstrated experimentally (Siviloglou et al., 2007). So far, Airy laser beams have found several applications for light trajectory control along ballistic-like paths (Hu et al., 2010), optical manipulation of particles (Christodoulides, 2008), navigation of long-range surface plasmons (Salandrino and Christodoulides, 2010), curved plasma filaments (Polynkin et al., 2009), abruptly autofocusing beams (Efremidis and Christodoulides, 2010) and others. As was later shown by Bandres (2009), Airy beams are a fundamental representative of the broader class of accelerating diffraction-free beams, another member being parabolic accelerating beams (Bandres, 2008). Notably, the trajectory of any accelerating and diffractionless beam can only be parabolic. However, due to their complex spectrum, accelerating beams, other than Airy, have to date remained mainly in the theoretical level.

The above review shows that (finite-energy) Bessel and Airy beams are to date the most popular and straightforward to implement forms of structured light waves with diffraction-resisting quality and non-accelerating or accelerating trajectories, respectively. With a Bessel beam, one can target a perfectly circular intensity lobe along a straight line and at distances much larger than implied by the diffraction length of a Gaussian beam with comparable width, while, with an Airy beam, one can steer the asymmetric Airy profile over many diffraction lengths along a parabolic trajectory. Thus, on the one hand, the fine symmetry of the Bessel profile is obtained at the cost of an exclusively straight trajectory, while, on the other hand, the curved trajectory of Airy beams is obtained at the cost of an asymmetric intensity distribution. Moreover, the curve of an Airy beam is limited to the parabolic law.

In view of these limitations, it is reasonable to ask if it would be possible to design hybrid beams that combine the best features of the two classes;

namely to design beams with the symmetry of the Bessel function that are also capable of self-accelerating similar to the Airy wavepacket. In addition, we may require that the trajectory is not limited to a parabola but it can be shaped rather arbitrarily. In this announcement we show that the answer to this question is affirmative.

Specifically, we present a technique for transforming a standard Gaussian laser beam into a Bessel-like beam capable of propagating along a prespecified path with arbitrary shape. The key idea is to phase-engineer the unmodulated wavefront so that the emitted rays form a continuum of conical ray bundles whose apexes (or foci) write the desired trajectory. The method is straightforward to implement experimentally since it only involves imprinting an appropriately computed phase pattern on the Gaussian wavefront using a spatial light modulator (SLM) or a hologram.

Interestingly, the possibility of Bessel beams with curved trajectories has recently been addressed in few works with the aim of producing spiralling and snaking Bessel beams (Jarutis et al., 2009); (Matijosius et al., 2010); (Morris et al., 2010). The method proposed in these works is quite approximate in the sense that the phase modulation of the beam is derived heuristically in a closed form and is not the one required to obtain a strict intersection of the ray cones exactly on the spiralling or snaking trajectory. Going beyond these fixed trajectories, we here address the problem of navigating Bessel beams along *arbitrary* trajectories in its most general formulation possible. We show how the correct phase pattern can be determined rigorously to ensure that the desired trajectory is actually a *focal* trajectory (or image curve) defined by the strict intersection of continuously expanding ray cones. Therefore, the present method can be used to design not only spiraling (helical) or snaking trajectories but any smooth curve. Moreover, a very clear Bessel profile is obtained that persists for much longer compared to the reported approximate approaches.

## 2 METHOD

To begin, assume that the initial distribution $u_0(\xi,\eta)$ of the optical field on the plane $z=0$ has the form of a slowly varying envelope $A(\xi,\eta)$ modulated by the phase $Q(\xi,\eta)$, where $\xi,\eta$ stand for the $x,z$ coordinates on that plane. For practical

laser beams, the transverse beam width (order of mm) is much larger than the optical wavelength (order of μm), hence the propagation of the optical field can be described very accurately by the scalar paraxial wave equation $2iu_z + u_{xx} + u_{yy} = 0$, whose solution is given by the Fresnel integral

$$u(x,y,z) = \iint \frac{u_0(\xi,\eta)}{2\pi i z} e^{i\frac{(x-\xi)^2+(y-\eta)^2}{2z}} \, d\xi d\eta \quad (1)$$

where $u_0(\xi,\eta) = A(\xi,\eta)\exp[iQ(\xi,\eta)]$ and the space coordinates are normalized by the arbitrary length scale $\chi$ in the transverse and by $k\chi^2$ in the longitudinal direction, $k = 2\pi/\lambda$ being the vacuum wavenumber. Note in Eq. (1) that the phase factor $\exp[i(k\ell)^2 z]$ has been omitted for convenience. Our goal is to determine the phase modulation $Q$ so that a focal track with a desired shape is created in $z > 0$. Parametrizing the trajectory of the focus with the propagation distance, this implies that, at any $z$, rays starting from the input plane must focus at the point $F(z) = (X(z),Y(z),z)$, where $X(z)$, $Y(z)$ are given functions. This strict requirement is a critical difference between our method and that used by Jarutis et al. (2009) or Morris et al. (2010). In these works the phase $Q$ was heuristically by assuming a segmentation of an axicon into displaced annuli, each of which produces a different part of the beam trajectory. In this way, $Q$ was defined in closed form but the rays do not actually intersect on the trajectory of the main lobe resulting in a not so clear Bessel-like profile.

Returning to our analysis, the equations of the rays are determined by the stationary points in the phase of the integrand in Eq. (1) and are given by

$$Q_\xi = \frac{x-\xi}{z}, \quad Q_\eta = \frac{y-\eta}{z} \quad (2)$$

where $Q_\xi, Q_\eta$ are the first partials of $Q$. Equations (2) imply that the ray starting from point $(\xi,\eta)$ on the input plane travels in the direction of vector $(Q_\xi,Q_\eta,1)$, i.e. it is determined by the gradient $\nabla_{\xi,\eta}Q$ of the input phase. According to our requirement, the point $F(z)$ must be the intersection of the bundle of rays starting from all points $(\xi,\eta)$ lying on a certain geometric locus $C(z)$ on the input plane (Fig. 1). This allows us to use Eq. (2) and rewrite the partial derivatives as

$$Q_\xi = \frac{X(z)-\xi}{z}, \quad Q_\eta = \frac{Y(z)-\eta}{z} \quad (3)$$

The correspondence between the point $(\xi,\eta)$ and the distance $z$, at which the rays emitted from the locus $C(z)$ intersect, can be thought to define a function of two variables $z(\xi,\eta)$ which makes the right-hand sides of Eqs. (3) functions of $\xi,\eta$. Equations (3) can then be used to determine the locus $C(z)$, which is essentially an *isoline* of function $z(\xi,\eta)$. To this end we note that, if $Q$ is twice continuously differentiable, its mixed partials must be equal (Clairaut's theorem), i.e. $Q_{\xi\eta} = Q_{\eta\xi}$ or explicitly from Eqs. (3)

$$\left[\xi - \xi_0(z)\right]z_\eta = \left[\eta - \eta_0(z)\right]z_\xi \quad (4)$$

where

$$\begin{aligned} \xi_0(z) &= X(z) - zX'(z) \\ \eta_0(z) &= Y(z) - zY'(z) \end{aligned} \quad (5)$$

and the prime denotes the derivative with respect to $z$. Equation (4) shows that the vector $(\eta - \eta_0(z), -\xi + \xi_0(z))$ is normal to the gradient $\nabla_{\xi,\eta}z$ and hence tangent to the local isoline, namely the locus $C(z)$. We may therefore write along $C(z)$

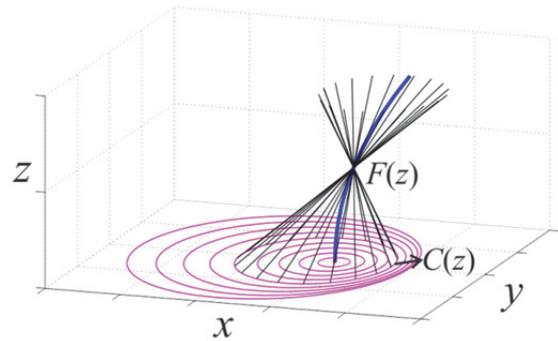$$\left[\xi - \xi_0(z)\right]d\xi + \left[\eta - \eta_0(z)\right]dh = 0.$$



Figure 1: The idea for producing diffraction-resisting laser beams with arbitrary trajectories: Conical ray bundles emitted from expanding circles on the input plane intersect on a predefined focal line.

Since $z$ is constant along an isoline, the above expression is an exact differential yielding:

$$\left[\xi - \xi_0(z)\right]^2 + \left[\eta - \eta_0(z)\right]^2 = r^2(z) \quad (6)$$

We therefore reach the conclusion that the geometric locus on the input plane of the starting points of the rays which intersect at $F(z)$, is a *circle* with center $(\xi_0(z), \eta_0(z))$ given by Eqs. (5) and radius $r(z)$, which is an arbitrary function for the moment. Equations (5) also show that the center of this circle is the point at which the tangent to the focal curve at $F(z)$ intersects the input plane. The analysis has therefore led to a clear physical picture which is illustrated in Fig. 1: with increasing $z$ as the beam propagates, a continuous focal line is created by the intersection of the bundles of rays emitted from circles $C(z)$ on the input plane with increasing radius $r(z)$ and a moving center $(\xi_0(z), \eta_0(z))$.

The radius $r(z)$ together with functions $X(z)$, $Y(z)$ determine the slope with which the rays interfere to create the focus $F(z)$ and hence the transverse field distribution around that point on the plane $z$. To see this explicitly, we take into account that each ray contributes a plane wave to the field in the region around $F(z)$. Defining the local coordinates around the focal point as $\delta x = x - X(z)$, $\delta y = y - Y(z)$, the field contribution of the ray from point $(\xi, \eta)$ of circle $C(z)$ is written in the paraxial approximation as

$$du = \exp\left[ iW(z) + \frac{i\left(X(z) - \xi, Y(z) - \eta\right) \bullet \left(\delta x, \delta y\right)}{z} \right] \quad (7)$$

where $\bullet$ denotes the inner product and

$$W(z) = Q(\xi, \eta) + \frac{\left(X(z) - \xi\right)^2 + \left(Y(z) - \eta\right)^2}{2z} \quad (8)$$

Note in Eq. (8) that the two phase terms yield a constant sum for all points $(\xi, \eta)$ of circle $C(z)$, which is a result of the stationarity [Eq. (2)] of the phase of the integrand of Eq. (1). Within the paraxial approximation, $W(z)$ is essentially the phase of the field contributed exactly on $F(z)$ by the ray emanating from $(\xi, \eta)$. Thanks to this remark, it is now easy to integrate the contributions $du$ over the circle $C(z)$. Introducing polar coordinates for convenience as $\delta x = \rho \cos\theta$, $\delta y = \rho \sin\theta$, and $\xi = \xi_0 + r\cos\varphi$, $\eta = \eta_0 + r\sin\varphi$, we find

$$\oint_C du = 2\pi \exp\left[ iW + i\frac{\left(X - \xi_0, Y - \eta_0\right) \bullet \left(\delta x, \delta y\right)}{z} \right] J_0\left(\frac{r\rho}{z}\right) \quad (9)$$

where the angular spectrum representation of the Bessel function has been used

$$J_0\left(r\rho/z\right) = 2\pi \int_0^{2\pi} e^{i\left(r\rho/z\right)\cos\varphi} \, d\varphi$$

Equation (9) shows that, at any distance, the optical field around the focus is distributed like a Bessel function modulated by a plane wave, which justifies the characterization of these waves as *Bessel-like*. Moreover, the result indicates explicitly the effect of the radius function $r(z)$ on the shape of the beam. To obtain a circular, Bessel-like beam with a lobe width that remains constant with $z$, and hence resists diffraction, the radius should be chosen to be proportional to the propagation distance or $r(z) = \beta z$, and then the lobe becomes proportional to $J_0(\beta\rho)$, where $\beta$ is the normalized transverse wavenumber. Without loss of generality, we can choose the transverse length scale $\chi$ so that $\beta = 1$ which we will assume in the numerical simulations section.

We now return to the main goal of our analysis which is the computation of the phase $Q(\xi, \eta)$. By virtue of Eq. (8), the problem is reduced to finding the phase $W(z)$ on the circle $C(z)$ that passes from the point $(\xi, \eta)$. For this purpose, we differentiate Eq. (8) with respect to $\xi$ (or $\eta$) and use Eqs. (3) and (6) to find after some algebra

$$W(z) = \frac{1}{2}\int_0^z \left\{ \left[X'(\omega)\right]^2 + \left[Y'(\omega)\right]^2 - \frac{r^2(\omega)}{\omega^2} \right\} d\omega \quad (10)$$

where we have arbitrarily set $W(0) = 0$. We have therefore ended up with a simple algorithm to compute $Q$ for given trajectory and radius functions $X(z), Y(z), r(z)$: For any point $(\xi, \eta)$ on the input plane, we first solve Eq. (6) for $z$ to find the isoline passing from that point, subsequently substitute into Eq. (9) to obtain $W(z)$ and finally obtain $Q(\xi, \eta)$ from Eq. (8). Thus, in order to design arbitrary trajectories, the input phase must be computed *numerically* through the above algorithm, while closed form solutions exist only when Eq. (6) can be explicitly solved for $z$. This is the key finding reported in this announcement.

Now let us consider a critical issue. It is important to see that the above algorithm is well defined only when Eq. (6) has a unique solution for

$z$, which means that circles $C(z)$ corresponding to different $z$ values must not intersect. Since the circles are the isolines of function $z(\xi,\eta)$, this requirement is ensured by the finiteness of the gradient $\nabla_{\xi,\eta}Q$. Differentiating Eq. (6) with respect to $\xi$ and $\eta$ we readily obtain

$$\nabla_{\xi,\eta}z = \frac{(\xi-\xi_0,\eta-\eta_0)}{rr'+(\xi-\xi_0)\xi'_0+(\eta-\eta_0)\eta'_0} \quad (11)$$

where from Eqs. (5) we have $\xi'_0 = -zX'', \eta'_0 = -zY''$. From the above equation, it is clear that the gradient remains finite if and only if the denominator does not vanish. This must hold for all points along $C(z)$ which we parametrize as $\xi = \xi_0 + r\cos\varphi$, $\eta = \eta_0 + r\sin\varphi$, with $0 \leq \varphi < 2\pi$. The denominator is then written

$$rr' - rz\sqrt{(X'')^2+(Y'')^2}\cos(\varphi-\theta)$$

where $\theta = \tan^{-1}(Y''/X'')$. Obviously, this expression remains nonzero when

$$r'(z) > z\sqrt{[X''(z)]^2+[Y''(z)]^2} \quad (12)$$

which is the sought condition. Note that, under this condition, the denominator is always positive which, from Eq. (11), means that the gradient $\nabla_{\xi,\eta}z$ points toward the exterior of the circle $C(z)$, thus verifying the expansion of the isolines with increasing $z$ (Fig. 1).

The condition of Eq. (12) defines an upper limit to the propagation distance $z_{\mathrm{m}}$ at which the focal curve can be created and, equivalently, a maximum circle $C(z_{\mathrm{m}})$ in the exterior of which the above definition of $Q$ fails. Indeed, consider for example the case of a power law trajectory lying on the plane $y = 0$, with $(X(z),Y(z)) = (\gamma z^\nu, 0)$. Substituting into Eq. (12) with $r(z) = z$, the maximum distance follows as $z_{\mathrm{m}} = [\gamma\nu(\nu-1)]^{-1/(\nu-1)}$, while from Eq. (5) it follows that the maximum circle is centered at $(\xi_0,\eta_0) = (\gamma(1-\nu)z^\nu_{\max}, 0)$ and has radius $r = z_{\mathrm{m}}$. Beyond the distance $z_{\mathrm{m}}$, the above analysis is not applicable and a different phase $Q$ must be defined in the exterior of the maximum circle. To this end, there is a certain choice that ensures two desired

properties: first, that $Q$ remains continuously differentiable on $C(z_{\mathrm{m}})$ and, second, that the beam preserves its diffraction-resisting quality for $z > z_{\mathrm{m}}$, although it stops accelerating. The choice is to continue the beam's trajectory along its tangent line at the ultimate point $F(z_{\mathrm{m}})$, i.e. as

$$\begin{aligned} X(z) &= X(z_{\mathrm{m}}) + X'(z_{\mathrm{m}})(z-z_{\mathrm{m}}) \\ Y(z) &= Y(z_{\mathrm{m}}) + Y'(z_{\mathrm{m}})(z-z_{\mathrm{m}}) \end{aligned} \quad (13)$$

where $z > z_{\mathrm{m}}$. It is then easy to see from Eq. (5) that the isolines of $z(\xi,\eta)$ for $z > z_{\mathrm{m}}$ are *concentric circles* with fixed center $(\xi_0(z_{\mathrm{m}}),\eta_0(z_{\mathrm{m}}))$ and increasing radius $r(z) = z$. The algorithm for computing $Q$ is the same with the $z \leq z_{\mathrm{m}}$ regime using however the new straight trajectory of Eqs. (13). Furthermore, for any point $(\xi,\eta)$ in the exterior of $C(z_{\mathrm{m}})$, Eq. (6) can be readily solved for $z$ giving

$$z = \sqrt{[\xi-\xi_0(z_{\mathrm{m}})]^2+[\eta-\eta_0(z_{\mathrm{m}})]^2}, \quad (14)$$

namely the distance between points $(\xi,\eta)$ and $(\xi(z_{\mathrm{m}}),\eta(z_{\mathrm{m}}))$ on the input plane. From Eq. (10) the corresponding $W(z)$ follows easily as

$$W(z) = W(z_{\mathrm{m}}) + \frac{[X'(z_{\mathrm{m}})]^2+[Y'(z_{\mathrm{m}})]^2-1}{2}(z-z_{\mathrm{m}}) \quad (15)$$

and finally the phase follows from Eq. (8)

$$\begin{aligned} Q(\xi,\eta) &= Q_0 - z + [\xi-\xi_0(z_{\mathrm{m}})]X'(z_{\mathrm{m}}) \\ &\quad + [\eta-\eta_0(z_{\mathrm{m}})]Y'(z_{\mathrm{m}}) \end{aligned} \quad (16)$$

where

$$Q_0 = W(z_{\mathrm{m}}) - \frac{z_{\mathrm{m}}\{[X'(z_{\mathrm{m}})]^2+[Y'(z_{\mathrm{m}})]^2-1\}}{2} \quad (17)$$

By defining the new coordinates on the input plane $(\xi',\eta') = (\xi-\xi_0(z_{\mathrm{m}}),\eta-\eta_0(z_{\mathrm{m}}))$, the phase from Eq. (16) can be equivalently written

$$Q(\xi',\eta') = Q_0 - \rho' + (\xi',\eta')\bullet(X'(z_{\mathrm{m}}),Y'(z_{\mathrm{m}})), \quad (18)$$

where $\rho' = [(\xi')^2+(\eta')^2]^{1/2}$. Therefore, the phase in the local polar coordinate system of point $(\xi(z_{\mathrm{m}}),\eta(z_{\mathrm{m}}))$ is the sum of a linear radial term and the phase of a plane wave. Such a phase is known to produce a modulated by a plane wave Bessel beam

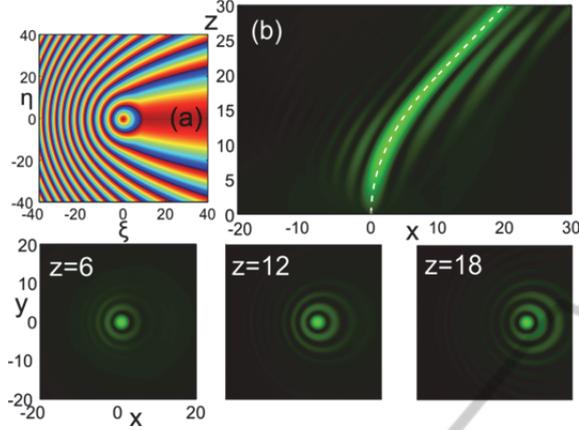that propagates along the straight line of Eq. (13).



Figure 2: A self-accelerating Bessel-like beam with the parabolic trajectory $x = 0.025z^2$. (a) Modulo-$2\pi$ input phase $Q$ (b) Amplitude evolution on the plane $y = 0$. The dashed line is the prespecified analytic trajectory. The bottom row shows images of the beam amplitude at different propagation distances.

This becomes evident if one recalls that the input condition $J_0(\rho)\exp(i\nu x)$ to the paraxial wave equation propagates as a tilted Bessel beam modulated by a plane wave, explicitly

$$J_0\left(\sqrt{(x-\nu z)^2 + y^2}\right)\exp\left(i\nu x - i\frac{(1+\nu^2)}{2}z\right).$$

We have therefore determined through rigorous analytical steps the phase required to produce a diffraction-resisting beam with a distant-independent Bessel profile capable of propagating along an arbitrary smooth trajectory. In the next Section we examine numerical simulations of several cases of the proposed beams as well as scenarios of self-reconstruction after distortions and propagation around obstacles.

# 3 NUMERICAL RESULTS

In Fig. 2 we design a Bessel-like beam with the parabolic trajectory $(X(z), Y(z)) = (0.025z^2, 0)$ in normalized coordinates lying on plane $y = 0$. The input Gaussian envelope has a full-width-at-half-maximum (FWHM) equal to 35 in normalized units. In (a), the phase modulation is shown as derived with the described algorithm and plotted as modulo-$2\pi$. Part (b) depicts the evolution of the field

amplitude on plane $y = 0$ as obtained via a second-order split-step Fourier simulation. Note how accurately the trajectory of the main lobe reproduces the analytically expected trajectory. For this example the maximum distance is $z_m = 20$, beyond which the beam continues along a straight line that matches the slope of the parabola at the transition point $(x, z) = (20, 20)$. The bottom row of Fig. 2 depicts snapshots of the beam's transverse profile at different distances and clearly verifies the expected Bessel-like pattern. The main lobe is remarkably symmetric and resistant to diffraction and fits almost perfectly the central lobe of $J_0(\rho)$, as predicted by Eq. (9). To the best of our knowledge, this is the first time that a self-accelerating optical beam with an almost perfect circular lobe is reported.

The clarity of the Bessel central profile observed in Fig. 2 and in the following simulations is a result of our strict requirement that the ray cones intersect exactly on the prespecified focal curve. The reader can contrast this with the simulation results for the spiraling Bessel beam in the context of the more approximate approach by Jarutis et al. (2009). It is also interesting to observe in Fig. 2 the weak asymmetric deformation of the surrounding rings toward the direction of the acceleration. When the beam enters its final straight track, the acceleration is zero and the intensity rings obtain again their symmetric profile.
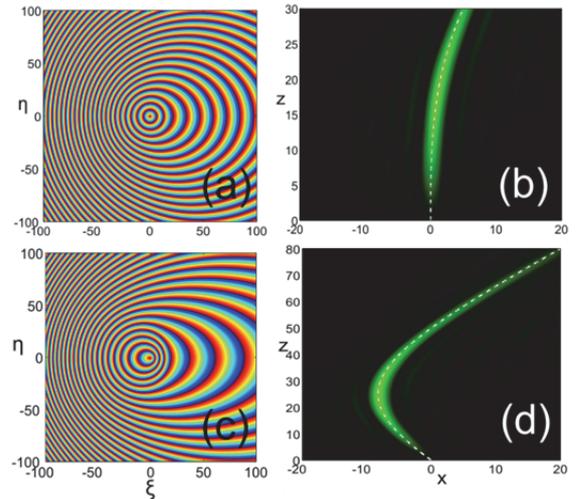


Figure 3: (a) Modulo-$2\pi$ input phase $Q$ and (b) amplitude evolution on the plane $y = 0$ for a beam with the cubic trajectory $x = 1.85 \times 10^{-4} z^3$. (c)-(d) The same results for a beam with the hyperbolic trajectory $x = 0.8(z^2 - 50z + 1250)^{1/2} - 800^{1/2}$.

Going beyond parabolic trajectories, Fig. 3 demonstrates the phase patterns and the evolution of beams with a cubic [(a)-(b)] and hyperbolic [(c)-(d)] trajectory. Note how the phase patterns appear as distorted versions of the perfect circular phase pattern $[Q(\xi,\eta) = -(\xi^2 + \eta^2)^{1/2}]$ of a Bessel beam, and that the direction of the distortion (stretching) is that of the acceleration of the focal curve. To our knowledge, this is the first report of beams with a Bessel-like profile that can follow trajectories designed at will. In some sense, the possibility of producing remarkably stable Bessel intensity lobes that can move along arbitrary curved paths in free space marries and at the same time enhances the best features of the standard Bessel and the standard accelerating beams.

Figure 4 shows another interesting possibility. Here the trajectory of the beam has been defined piecewise. Initially the beam propagates straight for a normalized distance 10 and subsequently detours along a half-period cosine path with length 50 and peak-peak distance 8 which guides it to its straight (and parallel to the initial) final path. Remarkable is the resistance that the beam shows against diffraction, as recorded in the amplitude snapshots at several distances [(b)-(f)]. At the initial part of the route [(a)], the beam cannot be distinguished from a standard Bessel beam. When the acceleration starts, a weak deformation of the rings is evident toward the negative $x$ axis [(c)]. At around $z = 35$, i.e. at the first quarter of the cosine period, the acceleration of the curve is zero and the deformation disappears [(d)]. Along the second quarter the acceleration changes sign and the rings start to weakly deform in the opposite direction [(e)]. Along its final straight track the beam recovers its perfectly symmetric Bessel profile [(f)]. It is thus interesting to observe the series of rings undergoing 'elastic' deformations under the acceleration experienced at different parts of the beam trajectory. Such and even more complicated configurations may be useful for navigating the optical power to avoid obstructions or carve elaborate paths with femtosecond pulses inside bulk glasses, as has recently been demonstrated using Airy-like beams (Mathis et al., 2012).

An example of a beam flowing around an obstruction is shown in Fig. 5. The obstruction is assumed to have the form of a cylindrical refractive index potential. The beam trajectory has been designed to obey the hyperbolic secant law with its maximum lateral shift occurring at the point where the potential barrier is centered along the z axis.
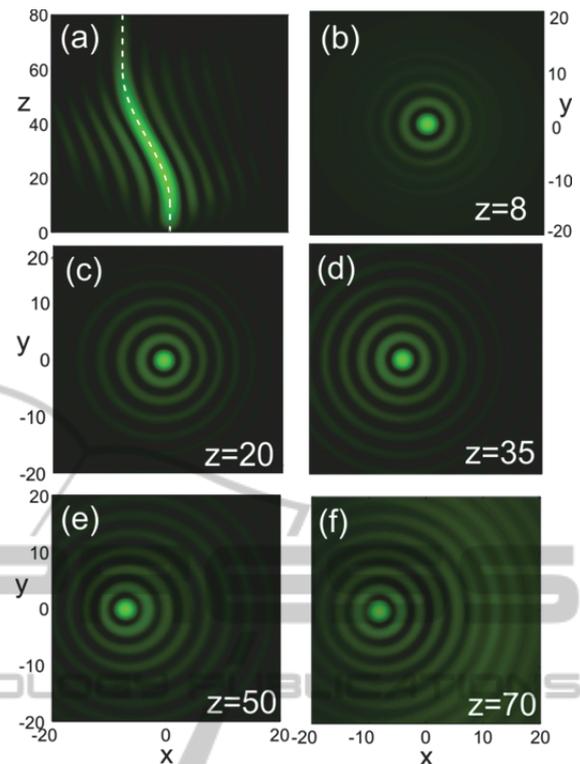


Figure 4: (a) Amplitude evolution on plane $y = 0$ for a beam with piecewise trajectory: $X(z) = 0$ for $0 < z < 10$, $X(z) = 4[\cos(\pi(z-10)/50) - 1]$ for $10 < z < 60$, and $X(z) = -8$ for $z > 60$. The analytic curve is shown with a dashed line. (b)-(f) Snapshots of the wave amplitude at different propagation distances.

Note in Fig. 5(a) how the beam avoids the potential essentially flowing around it thus minimizing the distortion of its profile [(b)] all along its route. Finally, as the trajectory tends asymptotically to the z-axis, an almost perfect symmetric Bessel beam profile is recovered [(c)].

Another beneficial feature of our hybrid beams is their ability to self-reconstruct their wavefront after distortions, even severe ones. This property is inherited by standard Bessel beams whose ray structure allows their field amplitude to be reconstructed after the beam has propagated for some sufficient 'healing' distance beyond the plane of distortion (Garces-Chavez et al., 2002). An analogue mechanism works with our arbitrary accelerating Bessel-like beams, where the beam profile at farther distances is due to the interference of rays emitted from distant points from the axis on the input plane (Fig. 1). Thus even if the central beam part is distorted or totally blocked, the beam eventually recovers its transverse pattern *and* trajectory.
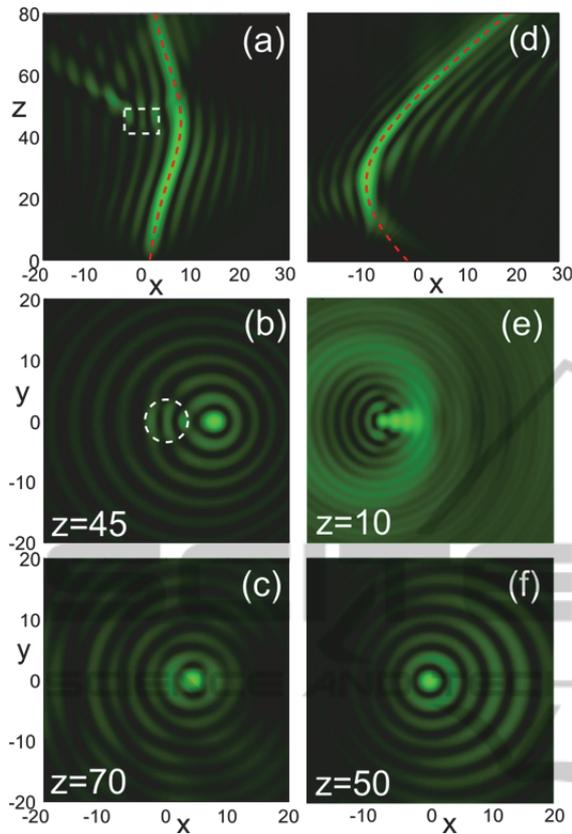
Figure 5: (a)-(c) Evolution and transverse amplitude snapshots at the indicated distances of a beam with a hyperbolic secant trajectory, in the presence of cylindrical potential (drawn with dashed line) with normalized amplitude 1. (d)-(f) Evolution and snapshots of the beam with the hyperbolic trajectory of Fig. 3(b) after blocking a central disk with radius 20 from the input condition.

A characteristic example is shown in Figs. 2(d)-(f) where the hyperbolic beam of Fig. 3(d) is left to propagate after blocking a large circular disk from the center of its input wavefront. We see that even if initially the beam profile [(e)] and trajectory [(d)] are significantly distorted, the wave manages to recover its structure after covering a healing distance of around 20 and write the intended hyperbolic track. Far beyond the healing point [(f)], the beam has fully recovered its profile and can hardly be distinguished from the undistorted beam of Fig. 3(d).

In a last example, Fig. 6 shows the case of a beam with a 3D trajectory that varies linearly in the $y$ and quadratically in the $x$ direction. The path of the main lobe has been recorded in (b). Parts (c) and (d) show how the images of the transverse beam profile follow the projection of the trajectory on the $xy$ plane. Beyond this example, the gamut of possibly interesting trajectories is virtually endless depending on the optical setting that the beam has to confront. We have thus managed to go beyond standard accelerating waves and design Bessel-like optical beams that can actually self-accelerate along arbitrary 3D paths.
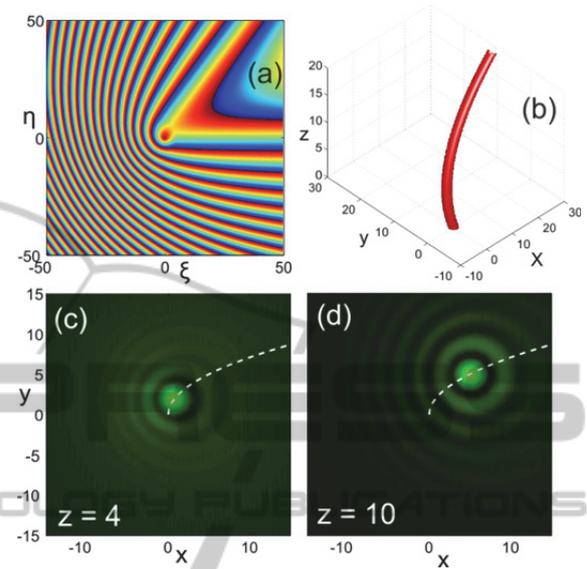


Figure 6: (a) Modulo-$2\pi$ input phase $Q$ and (b) track of the main lobe in 3D for a beam with trajectory $(X(z), Y(z)) = (0.05z^2, 0.5z)$. (c)-(d) Snapshots of the wave amplitude at different distances. The dashed line is the projection of the trajectory on the $xy$ plane.

## 4 CONCLUSIONS

We have proposed a method for generating diffraction-resisting, Bessel-like laser beams capable of propagating along arbitrary trajectories in free space. The key idea is to phase-modulate the wavefront of a standard Gaussian beam so that the emitted rays are grouped into conical bundles with expanding circular bases on the input plane that intersect continuously on a prespecified trajectory. Our work generalizes previous and more approximate efforts to manage the trajectories of Bessel beams along helical and snaking paths by setting a rigorous analytical framework for the systematic design of any beam trajectory. We have shown that, if the radius of these 'source' circles is chosen to be a linear function of the focal distance, the resulting focus has a distance-independent and hence diffraction-resistant Bessel function profile. The method can be used to design an inexhaustible gamut of trajectories, beyond the fixed parabolic law of Airy and Airy-related accelerating beams, such as

hyperbolas, general power laws, hyperbolic functions or even piecewise functions. We have demonstrated the feasibility of our method through several numerical simulations of paraxial optical beams. Such optical beams can be considered as advanced hybrids between nonaccelerating and accelerating diffractionless waves and, for that reason, can find extensive applications in optical tweezing, testing and microfabrication. Moreover, they can operate as curved photophoretic optical traps, capable of guiding particles around obstructions and exerting forces that are tunable in 3D.

## ACKNOWLEDGEMENTS

## REFERENCES

Andrews, D. L. (2008). *Structured Light and Its Applications*. Academic Press.

Arlt, J. and Dholakia, K. (2000). Generation of High-Order Bessel Beams by use of an Axicon. Opt. Comm., 177, 297-301.

Bandres, M. (2008). Accelerating Parabolic Beams. Opt. Lett., 33, 1678-1680.

Bandres, M. (2009). Accelerating Beams. Opt. Lett., 34, 3791-3793.

Bandres, M., Gutiérrez-Vega, J. and Chávez-Cerda, S. (2004). Parabolic Nondiffracting Optical Wave Fields. Opt. Lett. 29, 44-46.

Berry, M. and Balazs, N. (1979). Non-spreading Wave Packets. Am. J. Phys., 47, 264-267.

Christodoulides, D. (2008). Optical Trapping: Riding along an Airy Beam. Nat. Photon., 2, 652-653.

Durnin, J. (1987). Exact Solutions for Nondiffracting Beams. I. The scalar theory. J. Opt. Soc. Am. A, 4, 651.

Durnin, J., Miceli, J., Eberly, J. (1987). Diffraction-free Beams. Phys. Rev. Lett., 58, 1499-1501.

Efremidis, N., and Christodoulides, D. (2010). Abruptly Autofocusing Waves, Opt. Lett. 35, 4045-4047.

Garces-Chavez, V., McGloin, D., Melville, H., Sibbett, W., and Dholakia, K. (2002). Simultaneous Micromanipulation in Multiple Planes using a Self-Reconstructing Light Beam," Nature, 419, 145-147.

Grier, D. G. (2003). A Revolution in Optical Manipulation. Nature, 424, 810-816.

Gutiérrez-Vega, J., Iturbe-Castillo, M. and Chávez-Cerda, S. (2000). Alternative Formulation for Invariant Optical Fields: Mathieu Beams. Opt. Lett., 25, 1493-1495.

Herman, R. and Wiggins, T. (1991). Production and Uses of Diffractionless Beams. J. Opt. Soc. Am. A, 8, 932-942.

Hu, Y., Zhang, P., Lou, C., Huang, S., Xu, J. and Chen, Z. (2010). Optimal Control of the Ballistic Motion of Airy Beams. Opt. Lett., 35, 2260-2262.

Jarutis, V., Matijosius, A., Di Trapani, P. and Piskarskas, A. (2009). Spiraling Zero-Order Bessel Beam. Opt. Lett., 34, 2129-2131.

Mathis, A., Courvoisier, F., Froehly, L., Furfaro, L., Jacquot, M., Lacourt, P.A., Dudley, J.M. (2012). Micromachining along a Curve: Femtosecond Laser Micromachining of Curved Profiles in Diamond and Silicon using Accelerating Beams. Appl. Phys. Lett., 101, art. no. 071110.

Matijosius, A., Jarutis, V. and Piskarskas, A. (2010) Generation and Control of the Spiraling Zero-Order Bessel Beam. Opt. Express, 18, 8767-8771.

McGloin, D. and Dholakia, K. (2005). Bessel Beams: Diffraction in a New Light. Contemp. Phys., 46, 15-28.

Morris, J. E., Čižmár, T., Dalgarno, H.I.R., Marchington, R.F., Gunn-Moore, F. J., and Dholakia, K. (2010). Realization of Curved Bessel Beams: Propagation around Obstructions. J. Opt., 12, 124002.

Polynkin, P., Kolesik, M., Moloney, J., Siviloglou, G., Christodoulides, D. (2009). Curved Plasma Channel Generation using Ultra-Intense Airy Beams. Science, 324, 229-232.

Salandrino, A. and Christodoulides, D. (2010). Airy Plasmon: A Nondiffracting Surface Wave. Opt. Lett., 35, 2082-2084.

Siviloglou, G. and Christodoulides, D. (2007). Accelerating Finite Energy Airy Beams. Opt. Lett., 32, 979-981.

Siviloglou, G., Broky, J., Dogariu, A. and Christodoulides, D. (2007). Observation of Accelerating Airy Beams. Phys. Rev. Lett., 99, 213901.